Identification of sub-μs isomeric states in the odd-odd nucleus ^{178}Au

S. A. Gillespie,[1,2,*] A. Stott,[1] A. N. Andreyev,[1,3] J. G. Cubiss,[1] M. Al Monthery,[1] C. J. Barton,[1] S. Antalic,[4] K. Auranen,[5,†] H. Badran,[5] D. Cox,[5,‡] T. Grahn,[5] P. T. Greenlees,[5] A. Herzan,[5,§] E. Higgins,[6] R. Julin,[5] S. Juutinen,[5] J. Klimo,[7] J. Konki,[5,‖] M. Leino,[5] M. Mallaburn,[5] J. Pakarinen,[5] P. Papadakis,[5,6] J. Partanen,[5] P. M. Prajapati,[7] P. Rahkila,[5] M. Sandzelius,[5] C. Scholey,[5] J. Sorri,[5] S. Stolze,[5] R. Urban,[7] J. Uusitalo,[5] M. Venhart,[7] and F. Wearing[6]

[1]*Department of Physics, University of York, York YO105DD, United Kingdom*
[2]*TRIUMF, Vancouver, British Columbia, Canada V6T 2A3*
[3]*Advanced Science Research Center, Japan Atomic Energy Agency, Tokai-mura, Japan*
[4]*Department of Nuclear Physics and Biophysics, Comenius University in Bratislava, 84248 Bratislava, Slovakia*
[5]*Department of Physics, University of Jyväskylä, P.O. Box 35, FI-40014 Jyväskylä, Finland*
[6]*Oliver Lodge Laboratory, University of Liverpool, Liverpool L69 7ZE, United Kingdom*
[7]*Institute of Physics, Slovak Academy of Sciences, 84511 Bratislava, Slovakia*

(Received 24 September 2020; accepted 22 March 2021; published 2 April 2021)

The neutron-deficient gold ($Z = 79$) isotopes in the vicinity of the neutron midshell $N = 104$ provide prolific examples of shape coexistence and isomerism at low excitation energy. They can be probed via a number of different experimental techniques. In this study, two new isomeric states with half-lives of 294(7) and 373(9) ns have been observed in the neutron-deficient odd-odd nuclide ^{178}Au ($N = 99$) in an experiment at the RITU gas-filled separator at JYFL, Jyväskylä. This result was achieved due to the use of a segmented planar germanium detector with a high efficiency at low energies. By applying the recoil-decay tagging technique, they were assigned to decay to two different long-lived α-decaying states in ^{178}Au.

DOI: 10.1103/PhysRevC.103.044307

I. INTRODUCTION

The region surrounding the $Z = 82$ shell closure is well known for its exhibition of shape coexistence [1]. The neutron-deficient gold ($Z = 79$) isotopes are one of the earliest examples of this phenomenon, and have been studied by a variety of decay and in-beam nuclear spectroscopy techniques [2–10]; see also the recent review [11] and references therein. The ground state of gold nuclei displays a large increase in the mean-squared charge radius when approaching the $N = 104$ midshell [12,13]. While the gold isotopes with $A > 186$ possess weakly oblate ground states, $^{183-186}$Au are seen to have strong, prolate shapes. This sudden change in ground-state deformation has been related to the presence of $\pi i_{13/2}$, $\pi h_{9/2}$, and $\pi f_{7/2}$ intruder states at low energies, alongside spherical $\pi s_{1/2}$, $\pi d_{3/2}$, and $\pi h_{11/2}$ configurations [5,7,8]. Rotational bands built on top of these intruder states have been identified in several odd-A isotopes [2,14–16], with an observed parabolic trend in the bandhead energies as a function of neutron number (see for example, Fig. 1 in Ref. [5]).

Recently, a dedicated campaign of charge radii and magnetic dipole moment measurements was performed on the gold isotopes at ISOLDE [17]. In particular, the magnetic moments for ^{177,179}Au showed dominant $\pi s_{1/2}$ configurations with presumably near-spherical ground states [6], indicating an end to the region of strongly deformed ground states in gold nuclei. However, for ^{178}Au ($N = 99$), two α-decaying states were observed, with their magnetic moments best described by deformed Nilsson configurations [18]. The presence of these two deformed states in ^{178}Au, which is sandwiched between the near-spherical ^{177,179}Au nuclei, highlights the strong competition between spherical and deformed configurations in the lightest gold isotopes. One way to better understand the nature of these states is to study the excitations built on top of them.

In the ISOLDE study it was possible to identify and separate a low-spin ground state with $T_{1/2} = 3.4(5)$ s and a high-spin isomer with $T_{1/2} = 2.7(5)$ s in ^{178}Au, with most likely spin assignments of $I^\pi = (2^+\,3^-)$ and $(7^+\,8^-)$, respectively [18]. Fine-structure α-decay schemes were constructed for both states, with the most prominent lines appearing at $E_\alpha = 5922(5)$ keV, $I_{\alpha,\mathrm{rel}} = 86.49(9)\%$ for ^{178}Au^g, and $E_\alpha = 5925(7)$ keV [86.33(13)%] and 5977(10) keV [5.90(12)%] for ^{178}Au^m. In the case of ^{178}Au^m, the 5925-keV decay was observed in prompt coincidence with a strongly converted, 56.8-keV $M1$, γ-ray transition in ^{174}Ir.

The present work describes the first identification of two sub-μs isomeric states in ^{178}Au, performed in an experiment at the K-130 cyclotron at the Accelerator Laboratory of the

*stephen.gillespie.90@gmail.com
†Present address: Physics Division, Argonne National Laboratory, Argonne, Illinois 60439, USA.
‡Present address: Department of Physics, University of Lund, Lund, Sweden.
§Present address: Institute of Physics, Slovak Academy of Sciences, 84511 Bratislava, Slovakia.
‖Present address: CERN, CH-1211 Geneva 23, Switzerland.

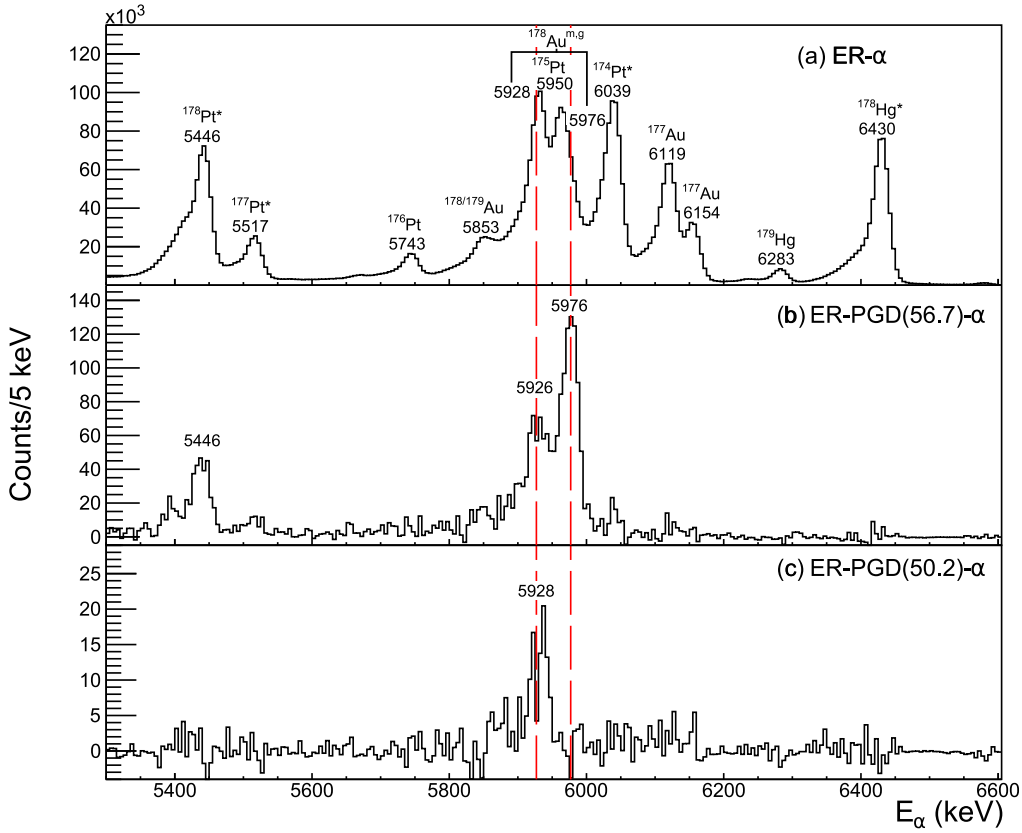

FIG. 1. (a): Energy spectrum of α decays, observed within 7 s of ER implantation in the DSSD. Peaks are labeled with their energies, in keV, and with the isotope they originate from. An asterisk marks the peaks used to calibrate the DSSD. (b) Same as (a), but a 56.7 ($\pm$1.0-keV energy window) γ decay must also be detected in the PGD within the time of ΔT(ER-PGD) = 0–1 μs. (c) Same time gates as (b), but with an energy gate on the 50.2 ($\pm$1.0-keV energy window) keV transition in the PGD.

University of Jyväskylä, Finland. Apart from providing further information on the complex decay scheme of this odd-odd nuclide, the new data could also help to clarify the so-far highly incomplete scheme for the α decay ^{182}Tl $\rightarrow$ ^{178}Au^{m,g}. Indeed, the recent laser-assisted α- and β-decay studies of ^{182}Tl at ISOLDE [19,20] identified two long-lived states in this nucleus, with several fine-structure α-decay branches and many prompt α-γ coincidences. However, most of them were not placed in the decay scheme of ^{182}Tl. This is due to complexity and multitude of closely lying low-energy excited states in the daughter nuclide ^{178}Au, which result from a variety of configurations expected to coexist in this nucleus [18].

II. EXPERIMENT

These data come from the same experiment in which a new 6.58(15)-μs isomeric state in ^{175}Ir was observed by our collaboration [21], therefore we refer the reader there for a detailed description of the experiment and the analysis techniques. A short description of the experiment will still be given here for completeness of the discussion.

A complete-fusion evaporation reaction ^{88}Sr + ^{92}Mo $\rightarrow$ ^{180}Hg* was exploited, in which ^{178}Au nuclei were produced in the 1p, 1n evaporation channel. A 381 MeV beam of ^{88}Sr impinged on a 600-μg/cm^2-thick self-supporting enriched ^{92}Mo target of 98% isotopic enrichment. Evaporation residues (ERs) were separated from the primary beam and fission products using the gas-filled separator RITU [22] and implanted into one of two double sided silicon detectors (DSSD), placed side by side, of the GREAT spectrometer [23]. Each DSSD has a thickness of 300 μm and consists of 60 $\times$ 40, 1 mm strips. In order to improve the overall energy resolution of the α-decay spectra, only strips with a resolution of $\leqslant$30 keV were considered in this analysis.

A segmented planar germanium detector (PGD), installed directly behind the DSSD, was used to detect x rays and low-energy γ rays at the focal plane of RITU. Energy calibration of the PGD was performed using standard calibration sources, ^{133}Ba, ^{152}Eu, and ^{241}Am. The data were collected and time-stamped using a total data readout data-acquisition system [24] and sorted with the GRAIN software [25].

III. DATA AND ANALYSIS

A. α-decay spectrum of the ^{88}Sr + ^{92}Mo $\rightarrow$ ^{180}Hg* reaction

Figure 1(a) shows a part of the energy spectrum of α decays, registered in the same pixel of the DSSD after an ER's implantation. A time window of ΔT(ER-α) = 7 s was used, which comprises $\approx$2 half-lives of ^{178}Au^{m,g}. The observed α-decay peaks originate from a multitude of nuclei directly produced in different xn, pxn, and αxn channels of

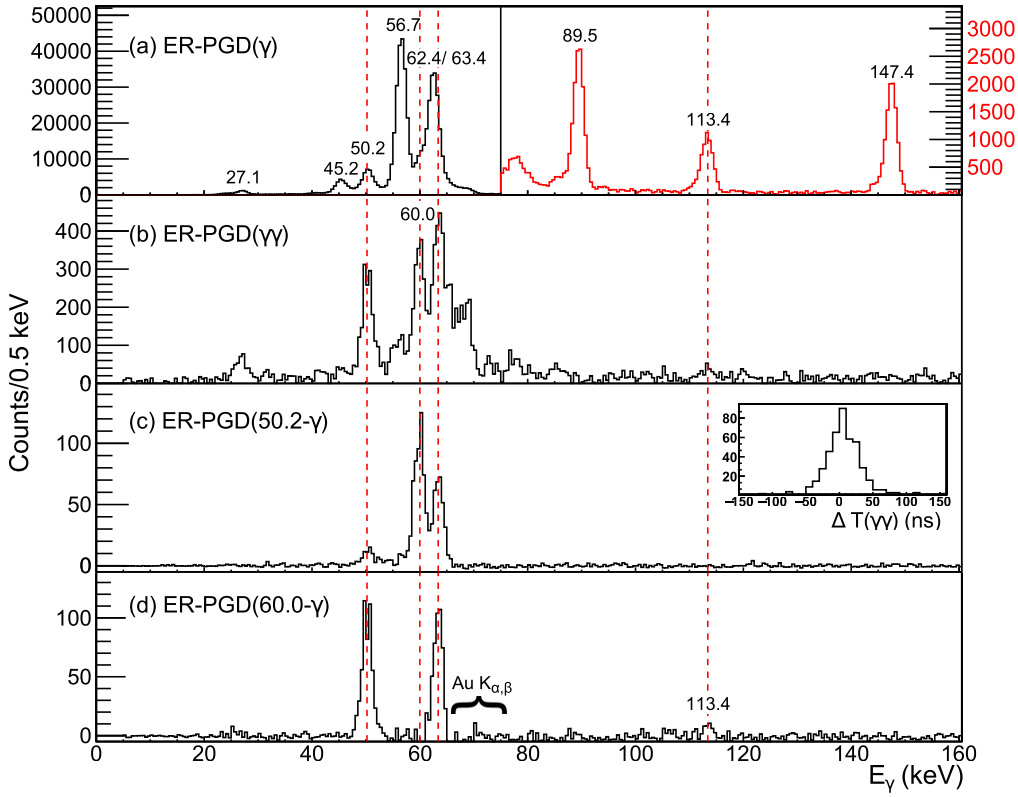

FIG. 2. (a) Recoil-gated singles γ-ray spectrum, observed in the PGD within the time of ΔT(ER-PGD) = 0–1 μs of the ER implantation in the DSSD. The centroids of the peaks are obtained from fits and labeled with their energies in keV. Note the change of the Y-axis scale from 80keV on. (b) Projection of a recoil-gated PGD($\gamma\gamma$) matrix for events with the prompt time condition $\Delta t(\gamma$-$\gamma) \leqslant 70$ ns, (c) Same as (b), but with an energy gate of $\pm$1 keV applied on the 50.2-keV transition. (d) Same time gates as (c), but with an energy gate of $\pm$1 keV on the 60.0-keV transition. The inset to (c) shows the time distribution for the 50.2–63.4-keV coincident events.

the measured reaction, and also from their daughter nuclides. Calibration of the DSSD was performed using known decays of ^{178}Pt [5446(3) keV], ^{177}Pt [5517(4) keV], ^{174}Pt [6039(3) keV], and ^{178}Hg [6430(6) keV], whose energies were taken from ENSDF [26]. The remaining peak energies seen in Fig. 1(a) are in good agreement with the known values with the exception of the decay of ^{176}Pt. We measure an energy of 5743(8) keV compared to the evaluated value of 5753(3) keV [26]. We note, however, that our value agrees within one sigma with the two most recent measurements, 5748(4) [27] and 5741(8) [28], included within the evaluated energy.

In contrast to the ISOLDE study of ^{178}Au^{m,g} [18], the separation of α decays from the isomeric and ground states is not possible in our study, if one relies only on the ER-α correlations in Fig. 1(a). This limitation is because their α-decay energies and half-lives are quite similar. Furthermore, in Fig. 1(a), the strongest α decays of ^{178}Au partially overlap with the dominant 5950(5)-keV α decay of ^{175}Pt (tabulated value 5948(4) keV [26]). The latter was proved based on the observation of α(5950 keV)-γ(76.8 keV) coincidence events belonging to the decay of this nuclide [26], this analysis will be discussed elsewhere [29].

Nevertheless, anticipating the followup discussion in Sec. III B 2, the strongest α decays of both states in ^{178}Au at 5928(10), 5926(8), and 5976(8) keV could be distinguished via coincidences with γ transition [Figs. 1(b) and 1(c)], which match well to the decays attributed to two α-decaying states in ^{178}Au [18].

B. Identification of submicrosecond isomeric states in ^{178}Au

1. Recoil-PGD singles

The μs isomeric transitions on top of both α-decaying states in ^{178}Au were identified based on the analysis of recoil-gated γ-ray spectra measured in the PGD. As the time of flight of recoils through RITU is ≈400 ns, only isomeric states of nuclei with half-lives comparable to (or longer than) this value can survive until the implantation in the DSSD. Their subsequent γ decay can then be measured by the PGD, within a specific time interval, ΔT(ER-PGD), following the implantation of an ER in the DSSD. In this work, such γ-ray events are called "recoil-gated isomeric decays" and denoted as ER-PGD.

Figure 2(a) shows the recoil-gated isomeric γ-ray PGD spectrum with the requirement that events occur within the time interval of ΔT(ER-PGD) = 0–1 μs. The 27.1(2), 62.4, and 89.5(2) keV transitions are known decays of the 89.5-keV 328(2)-ns isomeric state in ^{179}Au [16]. The 45.2(2)-keV transition originates from a 6.58-μs isomeric state in ^{175}Ir [21]. The 147.4(4)-keV decay belongs to ^{177}Pt [30]; its improved

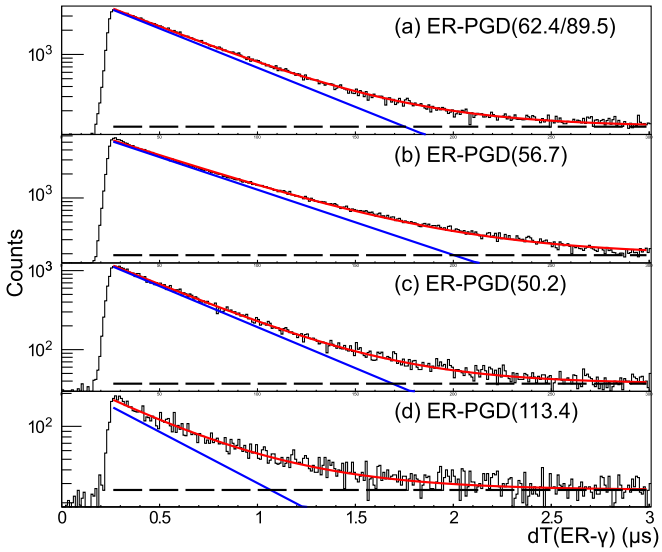

FIG. 3. (a) Decay curve for the sum of data for the 62.4- and 89.5-keV transitions in ^{179}Au. The fit (in red) consists of an exponential function (in blue) and a constant background (dashed black). (b) Same as (a), but for the 56.7-keV transition in ^{178}Au. (c) Same, but for the 50.2-keV transition in ^{178}Au. (d) Same, but for the 113.4-keV transition in ^{178}Au.

half-life of 2.35(4) μs was reported in [21]. The remaining peaks at 50.2(2), 56.7(2), and 113.4(4) keV are due to decays from two new sub-μs isomeric states in ^{178}Au, as discussed below.

We deduced the half-lives of the known and new isomeric transitions from the fits of the time distributions between an ER implantation in the DSSD and the detection of the isomeric γ-ray transitions in the PGD; see Fig. 3. The fit function consists of an exponential function and a constant background, used to account for γ rays not correlated to an ER and which have a flat time distribution. The method was first confirmed by measuring the half-life of the known 89.5 keV isomeric state in ^{179}Au [16]. From the combined statistics of the 62.4- and 89.5-keV transitions, as shown in Fig. 3(a), a value of $T_{1/2}$(89.5-keV state) = 322(9) ns was determined, which is consistent with the previous value of 328(2) ns. As will be proved in Sec. III B 3, the peak denoted as "62.4/63.4" in Fig. 2(a) is a convolution of the dominant 62.4-keV transition from ^{179}Au and a much weaker 63.4(2)-keV transition from ^{178}Au. Therefore, to further minimize a small possible lower-energy tail from the 63.4-keV decay to the 62.4-keV transition in the the half-life determination procedure, an energy gate of 61.4–62.6 keV was applied for the latter decay.

Using the same procedure for the newly observed strong 56.7-keV transition, a half-life value of $T_{1/2}(56.7\ \text{keV}) = 373(9)$ ns was deduced [Fig. 3(b)]. Similarly, values of $T_{1/2}(50.2\ \text{keV}) = 285(18)$ ns and $T_{1/2}(113.4\ \text{keV}) = 319(20)$ ns were determined, as shown in Figs. 3(c) and 3(d), respectively. The two values are consistent with each other within their uncertainties, and as will be shown in Sec. III B 3, both transitions will be assigned as originating from the same isomer. Therefore, we combined their respective statistics to a single fit, which resulted in a value of $T_{1/2}(50.2/113.4) = 294(7)$ ns.

2. Recoil decay tagging

The assignment of the new transitions to ^{178}Au was performed with the recoil decay tagging (RDT) method by searching for events of the type [ER-PGD]-α. Here, the ER-PGD event, with an energy gate on a specific isomeric γ-ray transition, should be observed within ΔT(ER-PGD) = 0–1 μs and be correlated to the α decay in the DSSD within ΔT(ER-α) = 7 s.

Figure 1(b) shows the same α-decay spectrum as Fig. 1(a), but with an additional energy gate of $\pm$1 keV on the 56.7-keV isomeric decay. Two α-decay peaks with energies of 5926(8) and 5976(8) keV are seen, which match well to the strongest decays of ^{178}Au^{m} [18]. Therefore we assign the 373-ns, 56.7-keV transition as feeding to the high-spin α-decaying isomer of ^{178}Au; see Fig. 4(b).

We note, however, that the intensity ratio of the two α decays in Fig. 1(b) is different from that measured at ISOLDE; the latter values are given Fig. 4(b). This difference may be explained by the fact that, in the RITU experiment, the ERs are implanted directly in the DSSD at a depth of several microns. Prompt and strongly converted γ-ray transitions, following α decay, will lead to an $\alpha + e^-$ summing effect, where both α particle and the coincident conversion electron are registered in the same strip of the DSSD. This is the case for the prompt α(5926)-γ(56.8) coincidences, whereby the $M1$ 56.8-keV has a large total theoretical conversion coefficient of $\alpha_{\text{tot,th}} = 6.78$ [31], with a dominant L- and M-shell internal conversion. The latter produces 42.5- and 53.4-keV conversion electrons, respectively, whose summing in the DSSD with the energy of the 5926-keV decay results in the depletion of its intensity and the enhancement of the summing peak at $\approx$ 5976 keV. A similar effect also happens in the ISOLDE experiment [18], but with a much reduced summing efficiency. This is because, at ISOLDE, ^{178}Au nuclei are implanted in a carbon foil placed in front of the silicon detector, thus the $\alpha + e^-$ summing is strongly reduced; see the GEANT simulations presented in [18].

By applying a $\pm$1-keV energy gate on the 50.2-keV decay, the spectrum shown in Fig. 1(c) was obtained, in which a single peak at 5928(10) keV is seen. As this energy corresponds to the 5922-keV decay of ^{178}Au^{g} [18], we establish that the 50.2-keV decay originates from the 294-ns isomeric state, whose decay eventually proceeds to the ground state of ^{178}Au. However, we note already here that the decay of the 294-ns state involves several transitions in a cascade, with 50.2-keV being one of them; see the discussion in Sec. III B 3 and the decay scheme in Fig. 4(a). The statistics for the 113.4-keV transition are too low to perform the RDT analysis, but its placement in the decay scheme can be done based on the γ-γ coincidence analysis in the PGD in Sec. III B 3.

The weak 5446(8)-keV peak in Fig. 1(b) is from the decay of ^{178}Pt, which originates from the β^+/EC decay of ^{178}Au^{m,g} ($b_\beta \approx 84\%$ in both cases [18]; see Fig. 4).

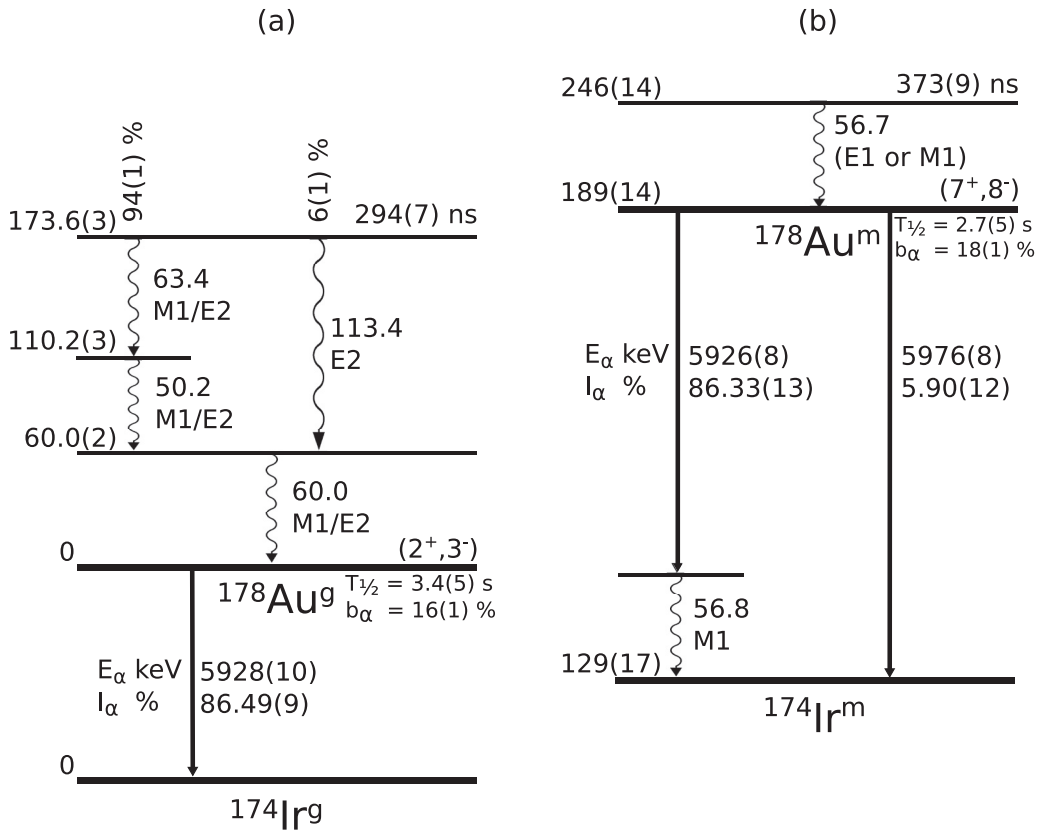

FIG. 4. (a) Proposed decay schemes of the new 294-ns isomeric state in ^{178}Au, deexciting to the low-spin ^{178}Au^{g} α/β-decaying state. (b) Decay scheme of the new 373-ns isomeric state deexciting to the high-spin ^{178}Au^{m} α/β-decaying state. The quoted α-decay energies are from the present work, while the half-lives, α-decay branching ratios, relative intensities of α decays, and relative energies for ^{178}Au^{m,g} are from [18]. Only selected α decays relevant to this work and observed in our study are shown here, for the full α decays and intensities of all other (weaker) α decays, see [18].

3. Recoil-$\gamma\gamma$ analysis

Further analysis of the newly-observed isomeric transitions was performed by searching for recoil-gated prompt γ-γ coincident events in the PGD, which are denoted as ER-PGD($\gamma\gamma$) throughout the text; see Figs. 2(b), 2(c), and 2(d). The time condition of ΔT(ER-PGD) = 0–1 μs and a prompt time gate of $\Delta T(\gamma\text{-}\gamma) \leqslant 70$ ns were applied to produce all three spectra. Figure 2(b) shows the total projection of this γ-γ matrix.

The presence of the $\gamma\gamma$(27.1–62.4) coincident pairs in Fig. 2(b), originating from a known isomeric cascade in ^{179}Au [16], confirms the validity of our analysis. Apart from the 50.2-keV transition and a weak 113.4-keV transition, a new decay at 60.0(2) keV can also be seen.

Figure 2(c) shows a projection from the PGD($\gamma\gamma$) matrix with an energy gate of $\pm$1 keV on the 50.2-keV transition, whereby the above-mentioned 60.0-keV decay and a new 63.4(2)-keV decay are observed. Similarly, by applying a $\pm$1-keV gate on the 60.0-keV transition, the spectrum seen in Fig. 2(d) was produced, which shows the 50.2- and 63.4-keV transitions. The analysis of the time distributions between any two of the three transitions proved the prompt character of these coincidence pairs. As an example, the inset to Fig. 2(c) shows the time distribution for a pair of $\gamma\gamma$(50.2–63.4-keV) coincidences, in which only a symmetric narrow peak is seen. Similarly narrow and symmetric time spectra were also obtained for the 50.2–60.0- and 60.0-63.4-keV pairs, proving their prompt character. Based on the above analysis we conclude that the 50.2-, 60.0- and 63.4-keV decays establish a cascade of mutually coincident prompt transitions.

Importantly, a weak peak at 113.4 keV is also seen in Fig. 2(d), which is absent in Fig. 2(c). The latter suggests that the 50.2-keV transition is not in coincidence with the 113.4-keV decay. On the other hand, the sum of the 50.2- and 63.4-keV transitions is 113.6(4) keV. We therefore placed the 113.4-keV transition parallel to the 50.2–63.4-KeV cascade.

IV. DISCUSSION

A. Proposed level scheme

Based on the analysis presented in the previous sections, the decay schemes of the new sub-μs isomeric states in ^{178}Au were deduced, as shown in Fig. 4.

From the RDT analysis we determined that the 373-ns isomeric state deexcites via the 56.7-keV transition to the $I^{\pi} = (7^{+}, 8^{-})$ high-spin isomer in ^{178}Au, as shown in Fig. 4(b). The decay of the 294-ns isomeric state towards the $I^{\pi} = (2^{+}, 3^{-})$ ground state in ^{178}Au is more complicated due to the presence

TABLE I. Total experimental ($\alpha_{\mathrm{tot,exp}}$) and theoretical ($\alpha_{\mathrm{tot,th}}$) internal conversion coefficients and mixing ratios, $\delta(E2/M1)$, for listed γ decays, where available. The theoretical ICC values and mixing ratios were calculated with BrIcc [31]. Also shown are the reduced transition probabilities assuming that a given transition directly depopulates the isomeric state. Two scenarios, denoted as "Sc.1" and "Sc.2," are considered for the 56.7-keV decay, with a pure $M1$ or $E1$ multipolarity, respectively; see main text. The $B(M1)$ and $B(E2)$ values in the last two columns include the conversion, relative intensities (where relevant), and the mixing ratios, except for pure $E2$ 113.4-keV decay and 56.7-keV ($E1$ or $M1$) decay. The B values for mixed transitions were calculated within the framework described in Appendix I-1.1 of Ref. [33]. Unless noted otherwise the B values are calculated using the $\alpha_{\mathrm{tot,exp}}$ values.

E_γ (keV)	I_{Tot}	$\alpha_{\mathrm{tot,exp}}$	$\alpha_{\mathrm{tot,th}}(E1)$	$\alpha_{\mathrm{tot,th}}(M1)$	$\alpha_{\mathrm{tot,th}}(E2)$	$\delta(E2/M1)$	$B(E1)$ W.u.	$B(M1)$ W.u.	$B(E2)$ W.u.
294(7)-ns isomer									
50.2(2)	94(1)	19.3(25)	0.538(10)	9.74(18)	123(3)	0.30(4)		$2.5(4)\times10^{-5}$	0.39(6)
60.0(2)	100	10.4(12)	0.331(6)	5.77(10)	51.8(12)	0.34(5)		$2.7(4)\times10^{-5}$	0.37(6)
63.4(2)	94(1)	21.3(27)	0.285(5)	4.91(9)	39.7(9)	0.95(14)		$6.5(10)\times10^{-6}$	0.63(10)
113.4(4)	6(1)	3.11(7)[a]	0.302(5)	5.06(9)	3.11(7)				0.025(4)
373(9)-ns isomer									
56.7(2), Sc.1, $M1$	100	6(2)	0.386(7)	6.81(12)	68.1(16)			$4.6(15)\times10^{-5}$	
56.7(2), Sc.2, $E1$	100	0.386(7)[b]	0.386(7)				$2.3(4)\times10^{-6}$		

[a]For the pure $E2$ 113.4-keV decay, the experimental ICC coefficient $\alpha_{\mathrm{tot,exp}}$ is assigned to that of $\alpha_{\mathrm{tot,th}}(E2) = 3.11(4)$.
[b]In Sc. 2, the experimental ICC coefficient $\alpha_{\mathrm{tot,exp}}$ is equated that of $\alpha_{\mathrm{tot,th}}(E1) = 0.386(6)$.

of multiple transitions. Several possible relative orderings within the 50.2–60.2–63.4-keV cascade and of the 113.4-keV decay were considered, but based on the arguments presented below our preferred decay scheme is shown in Fig. 4(a).

B. Multipolarities of the 50.2-, 60.0-, 63.4-, and 113.4-keV transitions

Multipolarities of the 50.2-, 60.0-, and 63.4-keV transitions were deduced by measuring their total internal conversion coefficients (ICCs), $\alpha_{\mathrm{tot,exp}}$. For the 60.0-keV transition the ICC was calculated by comparing the number of 50.2-keV events in the ER-PGD singles spectrum [$N_\gamma(50.2)$, Fig. 2(a)], and the number of 50.2–60.0-keV coincidences in the ER-PGD($\gamma\gamma$) spectrum [$N_{\gamma\gamma}(50.2\text{–}60.2)$, Fig. 2(c)]. The ICC of the 60.0-keV transition is calculated using the following equation:

$$\alpha_{\mathrm{tot,exp}}(60.0) = \frac{N_\gamma(50.2)\times\epsilon(60.0)}{N_{\gamma\gamma}(50.2-60.0)} - 1, \qquad (1)$$

where $\epsilon(60.0)$ is the efficiency of the planar detector at 60.0 keV, taken from simulations [32]. For the efficiency we assume a 10% uncertainty, which also justifies approximating the efficiency for the detection of the coincident pair at 50.2 and 60.0 keV by the product of the respective single detection efficiencies. Using Eq. (1), a value of $\alpha_{\mathrm{tot,exp}}(60.0) = 10.4(12)$ was deduced. Similarly using this equation but for the 50.2–63.4-keV coincidences in Fig. 2(c), we obtain $\alpha_{\mathrm{tot,exp}}(63.4) = 21.3(27)$. A comparison of $\alpha_{\mathrm{tot,exp}}$ values with the theoretical conversion coefficients shown in Table I suggests a relatively weakly mixed $M1/E2$ assignment for the 60.0-keV transition [$\delta(E2/M1) = 0.34(5)$] and a strongly mixed $M1/E2$ assignment for the 63.4-keV transition [$\delta(E2/M1) = 0.95(14)$].

Comparing the intensities of the 50.2- and 63.4-keV transitions in Fig. 2(e) and accounting for the measured conversion coefficient of the 63.4-keV transition, we calculate $\alpha_{\mathrm{tot,exp}}(50.2) = 19.3(25)$. This value establishes its weakly mixed $M1/E2$ character, with $\delta(E2/M1) \approx 0.30(4)$.

The multipolarity of the 113.4-keV transition was established via the following procedure. Based on the level scheme shown in Fig. 4(a), the 113.4-keV transition must conserve parity, as it is parallel to the cascade of 50.2- and 63.4-keV transitions, which are both of the mixed $M1/E2$ character. This fact rules out an $E1$ multipolarity assignment for the 113.4-keV decay. Furthermore, Fig. 2(d) shows the presence of weak Au $K_{\alpha,\beta}$ x rays, which can only originate from the conversion of the 113.4-keV transition, due to specific gating conditions used to produce this spectrum. If the 113.4-keV transition had an $M1$ multipolarity, the expected amount of Au K x rays should have been at least ≈ 4 times larger than of the 113.4-keV transition itself in Fig. 2(d). This ratio is due to a rather large theoretical ICC, $\alpha_{K,\mathrm{th}}(113.4, M1) = 4.16(2)$, and also to accounting for a slightly larger PGD detection efficiency at x-ray energies in comparison to 113.4 keV. On the other hand, $\alpha_{K,\mathrm{th}}(113.4, \mathrm{E2}) = 0.573(3)$, would explain the low number of Au $K_{\alpha,\beta}$ x rays in Fig. 2(d). Therefore, we assigned a pure $E2$ character to the 113.4-keV decay.

The intensity ratio of the two parallel paths (50.2–63.0 keV and 113.4 keV), shown in Fig. 4(a) was determined by using the intensities of the 50.2- and 113.4-keV peaks from Fig. 2(a), corrected for their respective γ-ray detection efficiencies, internal conversion coefficients and mixing (in case of the 50-keV decay). The internal conversion was included by using theoretical total ICCs of $\alpha_{\mathrm{tot,th}}(113.4, E2) = 3.11(4)$ and $\alpha_{\mathrm{tot,exp}}(50.2) = 19.3(25)$.

C. Multipolarity of the 56.7-keV transition

The ICC for the 56.7-keV transition, feeding to $^{178}\mathrm{Au}^m$, was deduced based on the comparison of the respective numbers of 5926/5976-keV decays in the ER-PGD(56.7)-α spectrum in Fig. 1(b) and the ER-α spectrum in Fig. 1(a). Apart from the internal conversion of the 56.7-keV transition itself, the difference between the two numbers is due to three effects:

(i) The decay loss of the 56.7-keV isomeric state during flight time through RITU, which is easily accounted for based on reaction kinematics;
(ii) The PGD detection efficiency of the 56.7-keV state, which was taken from the simulations [32];
(iii) The amount of deexcitation which bypasses the 56.7-keV isomeric state directly to the α-decaying ^{178}Au^{m}. This bypass does not contribute to the ER-PGD(56.7)-α spectrum in Fig. 1(b), but respective α decays in the DSSD are seen in the ER-α spectrum Fig. 1(a). The latter will lead to a correction of the deduced conversion coefficient, because the higher the bypassing path is, the smaller the "true" ICC will become. The possible implications from the latter effect will be further discussed below.

For the simplicity of the present discussion, a detailed description of the whole procedure will be given elsewhere [29]; here we will only provide the most relevant details. The main difficulty of the applied method was the estimation of the number of 5926/5976-keV decays of ^{178}Au^{m} in the complex ER-α spectrum in Fig. 1(a), also by accounting for the $\alpha + e^{-}$ summing effect mentioned earlier. This step involved a procedure to account for the contamination from the α decay of ^{175}Pt, mentioned above, in particular its "main" 5950-keV decay, which strongly contributes to this region. This procedure also considered the relative production of ^{178}Au^{g,m}, deduced via the comparison of the relative production of a number of α-γ coincident pairs of ^{178}Au^{g,m}, which are known from [18].

Based on the above procedure, a value of $\alpha_{\mathrm{tot,exp}}(56.7) = 6(2)$ was deduced, which conservatively includes an uncertainty due to the estimation of the number of 5926/5976-keV events in Fig. 1(a), mentioned above. Two possible scenarios have to be considered to interpret this value, depending on the assumption on the amount of deexcitation which bypasses the 56.7-keV isomeric state directly to the α-decaying isomeric state in ^{178}Au, as mentioned earlier.

In the first scenario (Sc.1 in Table I), the measured $\alpha_{\mathrm{tot,exp}}(56.7) = 6(2)$ is considered to represent the "true" ICC. Its comparison to the theoretical ICC values of $\alpha_{\mathrm{tot,th}}(56.7, M1) = 6.81(11)$ and $\alpha_{\mathrm{tot,th}}(56.7, E2) = 68.1(12)$ in Table I would establish a pure $M1$ character for the 56.7-keV decay. In turn, this will require that most (if not all) of the deexcitation from the higher-lying excited states towards the α-decaying ^{178}Au^{m} state must proceed via the isomeric 56.7-keV decay.

In the alternative scenario (Sc.2 in Table I), we consider a possible deexcitation bypass of the 56.7-keV state, which will necessitate an $E1$ character for the 56.7-keV decay with a theoretical ICC of $\alpha_{\mathrm{tot,th}}(56.7, E1) = 0.386(6)$. The large difference between the experimental and the theoretical values will then require that most of the deexcitation path bypasses the 56.7-keV isomeric state directly towards the α-decaying ^{178}Au^{m} state. In this case, the amount of the bypass can be estimated from the expression

$$100\% - \frac{1 + \alpha_{\mathrm{tot,th}}}{1 + \alpha_{\mathrm{tot,exp}}}(56.7) \approx 80\%. \qquad (2)$$

To conclude the discussion of the ICC values, we note that we also applied the same method to the 50-keV transition, by comparing the respective numbers of 5928-keV events in the ER-PGD(50.2)-α spectrum in Fig. 1(c) and in the ER-α spectrum in Fig. 1(a). A value of $\alpha_{\mathrm{tot,exp}}(50.2) = 26(8)$ was deduced, which is consistent, within the uncertainty, to the $\alpha_{\mathrm{tot,exp}}(50.2) = 19.3(25)$ deduced via the ER-PGD($\gamma\gamma$) method in Sec. IV B. This would suggest that most (or all) of the deexcitation towards the α-decaying ^{178}Au^{g} state passes via the 294-ns isomeric state, decaying by the 63.4–50.2–60.0-keV cascade.

V. INTERPRETATION OF THE NEW ISOMERIC STATES IN ^{178}Au

A. 373-ns state

The above-mentioned scenarios Sc.1 and Sc.2 (see Table I) are further considered with an attempt to interpret the 56.7-keV isomeric transition.

In Sc.2, we assume an $E1$ character, which would naturally explain its isomeric character, as the reduced transition probability is $B(E1, 56.7) = 2.3(1) \times 10^{-6}$; see Sc.2 in Table I. This would be a typical hindered low-energy $E1$ decay, which often happens in this region of nuclei, with $B(E1)$ values in the range of 1×10^{-7} to 1×10^{-6} W.u. [34]. For example, the 62.4- and 89.5-keV $E1$ transitions are known to proceed from the 89.5-keV 328(2)-ns excited state in neighboring odd-A ^{179}Au [16]. Their respective reduced transition probabilities are $B(E1, 62.4) = 1.88(1) \times 10^{-6}$ and $B(E1, 89.5) = 5.3(2) \times 10^{-8}$ W.u.; see Table 1 of [16]. Another example of such hindered $E1$ decays is the 45.2-keV transition from the 6.58-μs state in ^{175}Ir, where a value of $B(E1, 45.2) = 2.12 \times 10^{-7}$ W.u. was recently deduced [21].

On the other hand, an assumption of a pure $M1$ multipolarity for the 56.7-keV decay would lead to its strong hindrance $B(M1) = 4.6(15) \times 10^{-5}$ W.u; see Sc.1 in Table I. Several strongly hindered $11/2^{-} \rightarrow 9/2^{-}$ $M1$ decays are known in the odd-A isotopes ^{185,187,189}Au, with a comparable hindrances of $B(M1) \approx 10^{-5}$ W.u.; see Fig. 1 of [35].

With the present data, we cannot choose between the two scenarios and provide a unique interpretation of the nature of this isomeric state. As mentioned above, a possible distinction between $E1$ and $M1$ multipolarities could be provided by experimentally establishing the amount of a bypass over this isomeric state in the decay pattern from the higher-lying excited states.

B. 294-ns state

The decay path of the 294-ns state is more complex and involves several transitions. Importantly, all pairs of 50.2-, 60.0-, and 63.4-keV decays show a prompt character in their mutual coincidences, an example is shown for the $\gamma\gamma$(50.2–63.4) pair in the inset to Fig. 2(c). This fact suggests that only one of these decays originates from the isomeric state, while the apparent isomeric half-lives of other transitions are determined just by the fact that they follow the initial isomeric decay.

The three transitions have a mixed $M1/E2$ character. It is instructive to first recall the Weisskopf half-life estimates for pure $M1$ and $E2$ multipolarities for such low-energy decays. Accordingly, typical half-lives of $\approx 10^{-11}$–10^{-10} s are expected for pure $M1$ 50–60-keV decays, while substantially longer values of a few hundreds of nanoseconds are expected for the $E2$ multipolarity. The latter provides a first clue to the possible nature of isomerism in this case, as a strong $E2$ component alone would be enough to produce an isomeric decay.

Among the three transitions, only the 63.3-keV decay has a strong $E2$ character, as evidenced by its experimental mixing ratio of $\delta(E2/M1) \approx 0.95(14)$ (Table I). This is about 3 times larger than the mixing ratios for other two decays. This ratio is further reflected in a larger $B(E2)$ transition strength for the 63.4-keV transition in comparison to the other two decays.

Therefore, in our opinion, the larger $E2$ component in the 63.4-keV transition is the reason for its isomeric half-life. Based on these grounds, we propose our preferred decay scheme for the 294-ns isomeric state as shown in Fig. 4(a), whereby the isomeric 63.4-keV decay is followed by a prompt 50.2–60.0-keV cascade.

C. Possible spin assignments for the new isomeric states

The nonobservation of the 173.6-keV delayed decay in our data suggests that the spin of the respective 294-ns 173.6-keV excited state should be different by at least three units of angular momentum relative to the most likely $I^\pi = (2^+, 3^-)$ ground state of ^{178}Au, proposed in [18]. Otherwise, for any $\Delta I \leqslant 2$ difference between the two states, a full energy decay would be expected, though it would be very weak and probably beyond the sensitivity of our experiment if it were an $M2$ decay. Overall, in the extreme case of a full alignment of the angular momenta of all three transitions (or accounting for an $E2$ for 113.4-keV decay), a spin value as high as 5–6 can be expected for the 294-ns state.

Based on either an $M1$ or $E1$ multipolarity for the 56.7-keV decay and the most likely assignment of $I^\pi = (7^+, 8^-)$ for ^{178}Au^m in [18], the possible spin of the 373-keV isomeric state can be 6,7,8,9. The lowest values of 6 and 7 should most probably be discarded, as otherwise it would open a possibility for the 373-ns state to decay to the 294-ns state or other lower-lying states on top of ^{178}Au^g. No evidence for such transitions was observed in our data.

VI. CONCLUSIONS AND OUTLOOK

In this work, the identification of two sub-μs isomeric states in ^{178}Au was presented. This measurement became possible due to the use of a unique segmented planar germanium detector of GREAT, which allowed the measurements of the low-energy γ rays. The high efficiency for the low-energy γ-γ coincidences in the PGD played a key role in the construction of the decays scheme of the 294-ns isomeric state. The application of the recoil-decay tagging method allowed us to establish the decay paths of these isomeric decays to specific α-decaying states in ^{178}Au. Reasons for the occurrence of the sub-μs isomeric states in this nucleus were proposed.

The establishment of the low-energy excitation scheme in ^{178}Au will pave the way for dedicated in-beam studies of this nucleus, based on the application of the isomeric-decay tagging technique and gating on the decays of sub-μs isomeric states. This possibility will allow a circumvention of the difficulties of using the RDT method for relatively long-lived α-decaying states with half-lives of ≈ 3 s in ^{178}Au.

Furthermore, the knowledge of the low-energy states in ^{178}Au will crucially help clarify the so-far poorly known α-decay scheme of the two long-lived states in the chain $^{182}\text{Tl} \rightarrow {}^{178}\text{Au}^{g,m}$. In particular, we notice that the existence of a 112.9(1)-keV transition in the decay of low-lying excited states in ^{178}Au was established in the α-decay study $^{182}\text{Tl} \rightarrow {}^{178}$Au in Ref. [19]. However, this transition was not yet placed in the decay scheme. It remains to be seen whether the 113.4(4)-keV decay observed in the present study is the same transition as seen in [19]. On the other hand, none of the 50.2-, 60.0-, 63.4-, and 56.7-keV decays assigned to ^{178}Au in the present work were reported in [19]. This could possibly be both due to their relatively large internal conversion coefficients and a much lower γ-ray detection efficiency of the setup used in [19]. However, we cannot rule out the possibility that the α decay of ^{182}Tl does not populate isomeric states seen in this investigation.

ACKNOWLEDGMENTS

The authors wish to thank the technical staff at the Accelerator Laboratory at the University of Jyväskylä for their excellent support. This work was supported by the United Kingdom Science and Technology Facility Council Grant No. ST/P003885/1, the EU 7th Framework Programme "Integrating Activities - Transnational Access," Project No. 262010 (ENSAR), the Academy of Finland under the Finnish Centre of Excellence Programme 2012–2017 (Nuclear and Accelerator Based Physics Programme at JYFL), the Slovak Research and Development Agency under Contracts No. APVV-15-0225 and No. APVV-14-0524, and the Slovak Grant Agency VEGA (Contracts No. 2/0129/17 and No. 1/0532/17). The authors also acknowledge the support of GAMMAPOOL for the loan of the JUROGAM detectors. A part of results in this study constitutes the Ph.D. thesis by A.S.

[1] K. Heyde and J. L. Wood, Rev. Mod. Phys. **83**, 1467 (2011).
[2] F. G. Kondev *et al.*,Phys. Lett. B **512**, 268 (2001).
[3] A. N. Andreyev *et al.*, Phys. Rev. C **80**, 024302 (2009).
[4] A. N. Andreyev *et al.*, Phys. Rev. C **90**, 044312 (2014).
[5] M. Venhart, F. A. Ali, W. Ryssens, J. L. Wood, D. T. Joss, A. N. Andreyev, K. Auranen, B. Bally, M. Balogh, M. Bender, R. J. Carroll, J. L. Easton, P. T. Greenlees, T. Grahn, P.-H. Heenen,

A. Herzáň, U. Jakobsson, R. Julin, S. Juutinen, D. Klč *et al.*, Phys. Rev. C **95**, 061302(R) (2017).
[6] J. G. Cubiss *et al.*, Phys. Lett. B **786**, 355 (2018).
[7] M. Venhart *et al.*, Phys. Lett. B **806**, 135488 (2020).
[8] M. Sedlák, Eur. Phys. J. A **56**, 161 (2020).
[9] A. E. Barzakh, D. Atanasov, A. N. Andreyev, M. Al Monthery, N. A. Althubiti, B. Andel, S. Antalic, K. Blaum, T. E. Cocolios, J. G. Cubiss, P. Van Duppen, T. D. Goodacre, A. de Roubin, Y. A. Demidov, G. J. Farooq-Smith, D. V. Fedorov, V. N. Fedosseev, D. A. Fink, L. P. Gaffney *et al.*, Phys. Rev. C **101**, 034308 (2020).
[10] A. E. Barzakh, D. Atanasov, A. N. Andreyev, M. A. Monthery, N. A. Althubiti, B. Andel, S. Antalic, K. Blaum, T. E. Cocolios, J. G. Cubiss, P. Van Duppen, T. D. Goodacre, A. de Roubin, G. J. Farooq-Smith, D. V. Fedorov, V. N. Fedosseev, D. A. Fink, L. P. Gaffney, L. Ghys, R. D. Harding *et al.*, Phys. Rev. C **101**, 064321 (2020).
[11] M. Venhart *et al.*, J. Phys. G **44**, 074003 (2017).
[12] C. Ekström, L. Robertsson, S. Ingelman, G. Wannberg, and I. Ragnarsson, Nucl. Phys. A **348**, 25 (1980).
[13] K. Wallmeroth, G. Bollen, A. Dohn, P. Egelhof, J. Grüner, F. Lindenlauf, U. Krönert, J. Campos, A. Rodriguez Yunta, M. J. G. Borge, A. Venugopalan, J. L. Wood, R. B. Moore, and H.-J. Kluge, Phys. Rev. Lett. **58**, 1516 (1987).
[14] W. F. Mueller *et al.*, Phys. Rev. C **59**, 2009 (1999).
[15] W. F. Mueller *et al.*, Phys. Rev. C **69**, 064315 (2004).
[16] M. Venhart *et al.*, Phys. Lett. B **695**, 82 (2011).
[17] A. N. Andreyev *et al.*, European Organization for Nuclear Research ISOLDE and Neutron ime-of-Flight Committee, Proposal P–319–ADD–1, 2013 (unpublished).
[18] J. G. Cubiss *et al.*, Phys. Rev. C **102**, 044332 (2020).
[19] C. Van Beveren *et al.*, J. Phys. G **43**, 025102 (2016).
[20] E. Rapisarda *et al.*, J. Phys. G **44**, 074001 (2017).
[21] S. A. Gillespie *et al.*, Phys. Rev. C **99**, 064310 (2019).
[22] M. Leino *et al.*, Nucl. Instrum. Methods Phys. Res., Sect. B **99**, 653 (1995).
[23] R. D. Page *et al.*, Nucl. Instrum. Methods Phys. Res., Sect. B **204**, 634 (2003).
[24] I. H. Lazarus *et al.*, IEEE Trans. Nucl. Sci. **48**, 567 (2001).
[25] P. Rahkila, Nucl. Instrum. Methods Phys. Res., Sect. A **595**, 637 (2008).
[26] NNDC Evaluated Nuclear Structure Data File (ENSDF), Accessed on March 10, 2021.
[27] J. D. Bowman, R. E. Eppley, and E. K. Hyde, Phys. Rev. C **25**, 941 (1982).
[28] R. D. Page, P. J. Woods, R. A. Cunningham, T. Davinson, N. J. Davis, A. N. James, K. Livingston, P. J. Sellin, and A. C. Shotter, Phys. Rev. C **53**, 660 (1996).
[29] A. Stott (unpublished).
[30] E. Hagberg *et al.*, Nucl. Phys. A **318**, 29 (1979).
[31] T. Kibédi *et al.*, Nucl. Instrum. Methods Phys. Res., Sect. A **589**, 202 (2008).
[32] A. N. Andreyev *et al.*, Nucl. Instrum. Methods Phys. Res., Sect. A **533**, 422 (2004).
[33] R. B. Firestone, *Table of Isotopes*, 8th ed. (Wiley-VCH, Weinheim, 1999), Vol. 2.
[34] P. M. Endt, At. Data Nucl. Data Tables **26**, 47 (1981).
[35] M. O. Kortelahti *et al.*, J. Phys. G **14**, 1361 (1988).